Title no. 92-S22

Performance of Hybrid Moment-Resisting Precast Beam-Column Concrete Connections Subjected to Cyclic Loading

by William C. Stone, Geraldine S. Cheok, and John F. Stanton

Test results of 10 hybrid precast concrete beam-to-column connections are presented. These tests constitute Phase IV of an experimental program on one-third-scale model precast moment-resisting connections conducted at the National Institute of Standards and Technology (NIST). The objective of the test program is to develop guidelines for the design of moment-resisting precast connections in regions of high seismicity. The hybrid connections consist of mild steel used to dissipate energy and post-tensioning (PT) steel used to provide the required shear resistance. Variables examined were the amount and type of mild steel (ASTM A 615). The amount of post-tensioning steel was varied to control the relative moment capacity contributed by the PT and mild steel. The specimens were subjected to reversed cyclic loading in accordance with a prescribed displacement history. Connection performances were compared to previous NIST tests based on energy dissipation capacity, connection strength, and drift capacity. Hybrid precast connection can be designed to match or exceed the performance of a monolithic connection in terms of energy dissipation, strength, and drift capacity.

Keywords: beam-column frame; concrete construction; cyclic loads; earthquake-resistant structures; joints (junctions); moments; post-tensioning; precast concrete.

Precast concrete frame construction is not used extensively in high-seismic regions of the United States, despite its potential benefits in construction speed and quality control. This is largely due to a lack of test data on precast moment-resisting frames, and to building codes (e.g., Uniform Building Code, ICBO 1991) based on historical data with cast-in-place construction. In most cases, the UBC monolithic detailing requirements cannot be easily achieved in a purely precast system. The result is that most precast structures can be made to satisfy the UBC in accordance with the requirements for an "undefined structural system." Such systems must be shown to be equivalent to monolithic systems by technical and test data, which establish the dynamic characteristics and demonstrate the lateral force resistance and energy absorption capacity. In addition, the UBC requires steel

reinforcement used to resist earthquake-induced forces to conform to ASTM 706 or A 615 Grades 40 and 60. These specifications exclude prestressing steel. Since the advantages of precasting and prestressing are interlinked, this limitation on prestressing seriously inhibits the use of precast concrete in high-seismic regions.

An experimental program to examine the behavior of one-third-scale model precast concrete beam-column connections subjected to cyclic inelastic loads was initiated at the National Institute of Standards and Technology (NIST) in 1987. The objective of the program was to develop recommended guidelines for the design of an economical precast moment-resisting beam-to-column connection suitable for use in regions of high-seismic risk. The basic concept uses post-tensioning steel to connect the precast elements and to provide the required shear resistance to the applied seismic, dead, and live loads.

Hybrid precast connections were studied during 1992 to 1994 in Phase IV of the NIST test program and are discussed in this paper. The hybrid connections contain mild steel and post-tensioning (PT) steel, both of which contributed to the moment resistance. In addition, the mild steel serves as an energy dissipator, and the post-tensioning clamps the beam against the column, allowing beam shear at the interface to be resisted by friction. Concern was raised that the shear resistance provided by this arrangement, without shear keys or corbels, would not be sufficient to resist the gravity forces in addition to the applied seismic forces. To address this con-

ACI member W. C. Stone obtained his BS and MS from the Rensselaer Polytechnic Institute and his PhD from the University of Texas at Austin. He is currently a research structural engineer at the National Institute of Standards and Technology, Gaithersburg, MD.

ACI member G. S. Cheok obtained her BS and MS degrees in civil engineering from the University of Maryland. She is currently a research structural engineer at the National Institute of Standards and Technology, Gaithersburg, MD.

ACI member John Stanton is an associate professor in the Civil Engineering Department at the University of Washington, Seattle. He is a member of joint ACI-ASCE Committee 550, Precast Concrete Structures. His research efforts have recently been concentrated on the analysis of articulated decks (including bridges), behavior of connections for precast concrete, behavior and analysis of unbonded prestressed systems, and elastomeric bearings for both bridges and seismic base isolation.
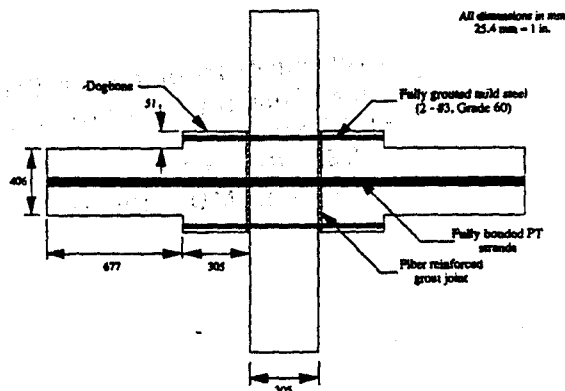
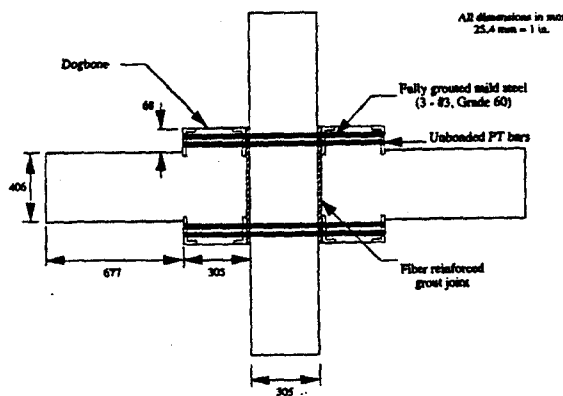Fig. 1—Basic details for Specimens I-P-Z4 and K-P-Z4

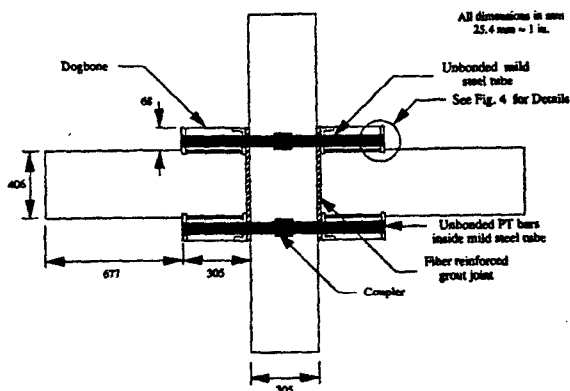Fig. 2—Basic details for Specimen J-P-Z4

Fig. 3—Basic details for Specimens L-P-Z4 A-C

cern, loads simulating gravity loads were applied to the beams.

Phase IV was divided into two subphases, A and B. In Phase IV-A (Cheok and Stone 1993), six tests were conducted on three exploratory designs. The objectives of this subphase were to test the hybrid concept and to explore different designs. The results were used to develop the specimen details for Phase IV-B (Cheok and Stone 1994). In Phase IV-B, four tests of "production" specimens were conducted. The beams and columns were fabricated by a precaster using standard fabrication methods and personnel. The connections were assembled and tested at NIST. The primary variables in this subphase were the amount and type of mild steel. The PT steel was located at the centroid of the beam. This location in Phases I through IV-A specimens produced the largest drift (relative story displacement) capacity prior to yielding of the PT steel.

Detailed results from Phases I, II, and III are found in reports by Cheok and Lew (1990, 1991), Cheok and Stone (1994), and in papers by Cheok, Stone, and Lew (1992), and by Cheok and Lew (1993). Specimens tested in Phases I through III were reinforced only with post-tensioning steel.

RESEARCH SIGNIFICANCE

The advantages of precast construction are inherent in the precast hybrid beam-column connections, as these are jointed connections as opposed to cast-in-place emulation-type connections. This study presents experimental data that show that the seismic performance of the hybrid beam-column connection is as good as or better than similar conventional cast-in-place connection.

SPECIMEN DESCRIPTION AND DETAILS

The results of the Phase I through III tests showed that both the connection strength and drift capacity of a precast connection can be made to match or exceed the performance of a corresponding monolithic connection. However, precast specimens reinforced with post-tensioning steel, alone, dissipated less energy than did the monolithic specimens. The main goal of the Phase IV tests was to evaluate the performance and, in particular, the damping characteristics of a post-tensioned precast connection that also contained elements designed to undergo cyclic yielding.

PHASE IV-A SPECIMENS

Three exploratory hybrid beam-column precast connections were designed and tested. The first design used fully bonded mild steel located in the top and bottom of the beam and fully bonded strands at middepth of the beam. The mild steel was placed at the outer edges of the beam to maximize the cyclic strains imposed on it, and the PT steel was placed at midheight of the beam to minimize the potential for yielding. Details are shown in Fig. 1.

A second design, shown in Fig. 2, used fully bonded mild steel and unbonded PT steel, both located at the top and bottom on the beam. Unbonded PT tendons were used to delay yielding of the PT steel.

The third design, shown in Fig. 3, employed replaceable steel. The ability to repair a structure by simply replacing the

failed steel elements instead of condemning it after an earthquake is economically attractive. This design used unbonded mild steel and PT steel collocated at the top and bottom of the beam. The strains in the PT steel were reduced by using unbonded PT tendons.

The first design used continuous PT strands that, in a prototype structure, would run the entire length of the building, whereas the second and third designs used short lengths of PT steel, which would be tensioned on a span-by-span basis. The advantage of using continuous PT is that it requires fewer anchorages and reduces labor. However, it constrains the construction sequence because the whole floor must be constructed prior to post-tensioning. The second and third designs remove this limitation, but the PT is more likely to yield by virtue of its location.

Design basis

The test specimens represented at one-third scale a beam-column joint from the bottom story of a prototype office structure. The basic structural system for this building was a perimeter moment-resisting frame. The prototype building was rectangular, 12 stories high, had plan dimensions of 30.48 x 60.96 m (100 x 200 ft, 6 bays x 12 bays), a 5.49-m (18-ft) column spacing, and a 3.96-m (13-ft) story height. The column dimensions were 914 x 914 mm (36 x 36 in).

The internal forces for the prototype were UBC (ICBO, 1988) Zone 4 loads, assuming $R_w = 12$. The beams in the prototype were 457 x 1219 mm (18 x 48 in.) and carried a factored moment M_u of 2440 kN-m (1800 kips-ft) at the column face. In a conventionally reinforced system, four No. 11 and three No. 10 bars top and bottom ($\rho = 1.27$ percent) would suffice. The column size was based on the UBC requirements for a strong column-weak beam design and on joint shear. A 914 x 914-mm (36 x 36-in.) column with 28 No. 14 bars ($\rho = 4.86$ percent) fulfilled this need. The properties of these prototype members were sufficiently close to those used in Phases I through III that comparisons were possible.

It was shown in Phase III that partial debonding of the PT steel improved the drift capacity prior to yield of the PT. Thus, unbonded and partially bonded PT steel was incorporated in the design of the Phase IV specimens. Currently, there is no accepted procedure for the design of a precast beam-column connection with mild steel and unbonded PT steel. The provisions of Chapter 18 of ACI 318 are inappropriate because they are empirical and are based on test data derived from beams and slabs that are significantly more slender than those in these tests, contain relatively little mild steel, and are subjected to monotonic loading. A computer program (Cheok and Stone 1993) was developed to compute the flexural and shear resistance of a hybrid beam at any imposed beam rotation. The strain in the unbonded part of the PT tendon was assumed to be equal over the entire unbonded length. The concrete compressive force was computed based on a triangular stress distribution ($0.5\ f_c'b_1c$) for steel strains less than or equal to yield and on the equivalent rectangular stress block ($0.85\ f_c'b\beta_1c$) for steel strains greater than yield.

The dimensions of the prototype beam were kept at 457 x 1219 mm (18 x 48 in.). The reinforcement was required to satisfy two criteria. The required shear force was based on a

moment equal to 3241 kN-m [2390 kips-ft, $\phi = 1$, $f_y = 517$ MPa (75 ksi)] and an applied dead load of 89 kN (20 kips)

$$\phi M_n \geq M_u = 2440 \text{ kN-m} \qquad (1a)$$

and

$$\phi V_n \geq V_u = 1557 \text{ kN} \qquad (1b)$$

An infinite number of combinations of PT steel and mild steel will satisfy the flexural requirement of Eq. (1a). The shear force was to be resisted by the shear friction, and this requirement imposes a lower limit on the PT force

$$\phi V_n = \mu A_{ps}f_{ps} + 0.4A_s'f_y \geq V_u \qquad (2)$$

where

$\mu = 0.6\lambda$ [ACI 318-89, Section 11.7.4.3]

$\lambda = 1.0$ for normal weight concrete

A_{ps} = area of PT steel

f_{ps} = nominal stress of PT steel

A_s' = total area of compression steel

f_y = yield stress of mild steel

The value of μ used was conservative, as the concrete surfaces on the beam and column were roughened and, therefore, a value of μ equal to 1 would have been permissible by ACI criteria. Eq. (2) must be satisfied at all times.

The beams in the Phase IV-A specimens had "dogbones" (Fig. 1)—over- and under-expanded flanges measuring 51 mm (2 in., Specimens I-P-Z4 and K-P-Z4) and 68 mm (2.67 in., Specimens J-P-Z4 and L-P-Z4 A-C) high and 305 mm (12 in.) long—which made the beams deeper at the column faces. The configuration and basic connection details are shown in Fig. 1 through 3. The mild steel extended from the end of one beam dogbone through the column to the end of the second beam dogbone. A horizontal failure plane occurring across the base of the dogbone was a possibility, due to the high shearing stress, so additional transverse reinforcement was included in the dogbone regions to prevent this mode of failure. The design of the reinforcement was based on that for corbels. In addition to the increased transverse reinforcement in Specimen J-P-Z4, steel angles were located at the ends of the dogbones (Fig. 2). These angles were considered necessary to provide confinement to the dogbone region, as the PT steel in Specimens J-P-Z4 and L-P-Z4 was also located in this section. Shear studs were welded to the angles farthest from the column face to prevent rotation of the angles. Also, No. 3 bars, 178 mm (7 in.) long, were welded to the angles closest to the column face to anchor the angles. A summary of the Phase IV specimens is given in Table 1. The reader should keep in mind that, for similitude, the prototype moments are scaled by a factor of $1/s^3$, where s is the scale factor.

Table 1—Description of NIST precast connections

Test phase	Specimen names	PT steel Type*	PT steel Bond†	PT steel, distance from extreme fiber d_p, mm	Length of debonded PT steel, mm	Mild steel Area, mm²	Mild steel Bond†
IV-A	I-P-Z4, K-P-Z4	S	F	254	—	142	F
IV-A	J-P-Z4	B	U	51	914	213	F
IV-A	L-P-Z4A	S	U	40	914	—	—
IV-A	L-P-Z4B	B	U	40	914	—	—
IV-A	L-P-Z4C	S	U	40	914	186	U
IV-B	M-P-Z4	S	P	203	1511	142	P
IV-B	N-P-Z4	S	P	203	1511	131	P
IV-B	O-P-Z4	S	P	203	1511	213	P
IV-B	P-P-Z4	S	P	203	1511	197	F

*B= high-strength bars; S = prestressing strands.
†F= fully grouted; P = partially grouted; U = unbonded.
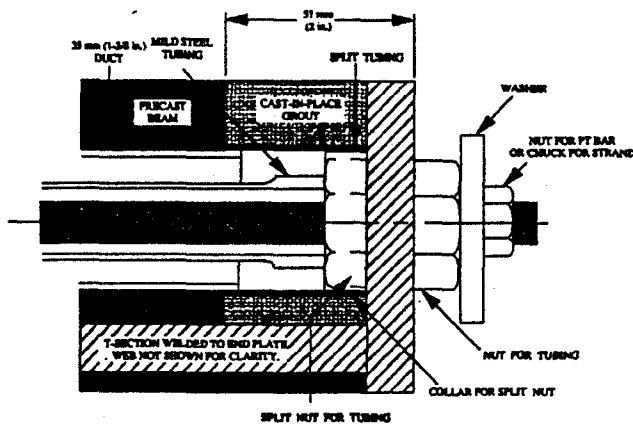25.4 mm = 1 in.

Fig. 4—Details of blockout in Specimen L-P-Z4 C

I-P-Z4 and K-P-Z4 specimen details

Specimens I-P-Z4 and K-P-Z4 (Fig. 1) were based on the first design concept: fully bonded mild steel located in the dogbones with fully bonded PT strands in the middle of the beam. The fully bonded PT provided resistance to corrosion and to progressive collapse in the improbable event of anchorage failure.

The mild steel in Specimen I-P-Z4 consisted of two No. 3, Grade 40 (f_y = 276 MPa) reinforcing bars. Their actual yield strengths were much higher than the specified 276 MPa (40 ksi).

Specimen K-P-Z4 was identical to Specimen I-P-Z4, except that Grade 60 (f_y = 414 MPa) reinforcing bars were used instead of Grade 40 (f_y = 276 MPa). Specimen K-P-Z4 was a retest of Specimen I-P-Z4, which had failed prematurely due to bond failure of the mild steel, as described later in this paper. The fully bonded prestressing tendons, three 13-mm (0.5-in.)-diameter seven-wire strands [f_{pu} = 1862 MPa (270 ksi)], were located at the center of the beam to delay yielding. For Specimens I-P-Z4 and K-P-Z4, the initial stress in the strands, after losses, was approximately 0.65 f_{pu}, resulting in an initial beam prestress of 5.0 MPa (725 psi) at the column face.

J-P-Z4 specimen details

Specimen J-P-Z4 (Fig. 2) was based on the second design: unbonded PT and fully bonded mild steels located in the dogbones. This design allows for construction to proceed on a span-by-span basis.

The high-strength bars, with a diameter of 11 mm (0.421 in.), were machined from 16-mm- (0.625-in.)-diameter Dywidag* bars [f_{pu} = 1034 MPa (150 ksi)]. The mild steel in this specimen comprised three No. 3 Grade 60 (f_y = 414 MPa) bars. The argument for using Grade 60 (f_y = 414 MPa) instead of Grade 40 (f_y = 276 MPa) was the greater availability of Grade 60 (f_y = 414 MPa) bars; the actual yield stress of a Grade 40 (f_y = 276 MPa) bar is often closer to 414 MPa (60 ksi). The initial axial beam prestress was 3.2 MPa (464 psi) for Specimen J-P-Z4. The initial stress in the high-strength bars after losses was approximately 0.65 f_{pu}.

L-P-Z4 specimen details

Specimen L-P-Z4 (Fig. 3) was constructed based on the third design: a replaceable system with unbonded PT and mild steels in the dogbones. This design also allows for construction to proceed on a span-by-span basis. The mild steel must be anchored so it can carry both tensile and compressive loads, and this was achieved by the system shown in Fig. 4.

In Specimens L-P-Z4 A-C, three variations of mild and PT steels were tested using the same beam and column by replacing the reinforcement after each test. The ability to replace both types of steel made the additional two tests possible. Specimen L-P-Z4 A was post-tensioned with two 11-mm- (⁷/₁₆-in.)-diameter seven-wire strands, Grade 270 (1862 MPa) top and bottom, and contained no mild steel. After the testing of L-P-Z4 A, the specimen was reassembled using two 11-mm- (0.421-in.)-diameter Dywidag bars in place of the strands. It was retested as Specimen L-P-Z4 B. The bars yielded at a lower drift capacity than the strands. On this basis, the third specimen, L-P-Z4 C, was post-tensioned with strand.

For the third specimen (LPZ4-C), tubing made of ASTM A 513 1026-type steel was used as the mild steel, and the PT steel was located concentrically inside the tubing, as shown

Table 2—Material properties

Specimen	f_c', MPa	Joint grout, MPa	Duct grout, MPa	f_y, MPa	f_u, MPa	f_{py}, MPa	f_{pu}, MPa
I-P-Z4	41	90	69	399	610	1738	1878
J-P-Z4	44	78	82	436	668	896	1000
K-P-Z4	37	72	64	436	668	1738	1878
L-P-Z4 C	38	72	—	538	628	1034	1103
M-P-Z4	47	73	78	422	673	1710	1868
N-P-Z4	47	78	73	517	686	1710	1868
O-P-Z4	47	73	73	523	780	1710	1868
P-P-Z4	47	75	77	431	695	1710	1868

1 MPa = 0.145 ksi.

in Fig. 3 and 4. Two 9.5-mm- ($^3/_8$-in.)-diameter seven-wire strands, Grade 270 top and bottom, were used to post-tension this specimen. The tubing was threaded at the ends where the wall was also thicker to insure that yielding occurred away from the threads. This was necessary to assure easy removal of the tubes. This type of tubing with upset threaded ends is readily available commercially as J-55 tubing and is commonly used in the oil industry. As the J-55 tubing was not available in the required size, 1026 tubing was used instead in Specimen L-P-Z4 C. The selection of 1026 steel tubing was based on the need to duplicate the stress-strain curve for the J-55 tubing, which would be used in a prototype specimen.

During the assembly of the specimen, the tube was threaded into a coupler embedded into the middle of the column. At the end of the dogbone, it was locked into place by two nuts, as shown in Fig. 4. The use of two nuts allowed the tube to carry both tensile and compressive forces. The interior nut was split into two C-shaped pieces and then held together by sliding a short length of tubing over it. This procedure was necessary to avoid having to thread the tube through the interior nut during construction. The PT steel for Specimen L-P-Z4 A-C was stressed to an initial value of $0.4 f_{py}$. The lower initial stress was used to increase the story drift at yield of the PT steel.

In the original design of Specimen L-P-Z4, six reinforcing bars were to be welded to the plates located at the ends of the dogbones. This was necessary to allow the mild steel tubes to carry compression forces. The reinforcing bars were to transfer the force from the front plate to the back angle, thereby anchoring the plate to the dogbone when the tube was subjected to compression. However, a structural steel T-section was used in the final one-third-scale model to avoid congestion in the blockout. The use of the T-section introduced a potential horizontal failure plane between the flange of the T-section and the beam. This is because the resistance to shear at the interface between the steel and concrete is much less than if the interface was monolithically cast concrete. To reduce the chances of this type of failure, four No. 4 bars, 178 mm (7 in.) long, were welded to the flange to act as shear studs. Two of these bars were bent at 90 deg, while the other two were straight.

Grouting process of Phase IV-A specimens

The ducts used in the specimens for the mild steel were 13-mm ($^1/_2$-in.) ID electrical conduit. The grout used in the construction joint between the precast beams and columns for all specimens was fiber reinforced. The construction joint widths were 8 mm ($^1/_3$-in.). Due to the small joint width and a desire to prevent corrosion of the fibers, nylon fibers, 13 mm ($^1/_2$-in.) long, were used. The fibers had a diameter of 584 µ m and a specific density of 1.16. The amount of nylon fibers used was 1.78 kg/m^3 (3 lb/yd^3) of concrete.

A neat cement grout with a water-cement ratio (w/c) of 0.35 was used to grout the bars into their ducts in Specimen I-P-Z4. However, this specimen experienced premature bond failure of the mild steel, as discussed later in this paper. Although the neat cement grout was not the cause of the failure, it was felt that the use of a commercially available grout would be more representative of field conditions. Therefore, a grout with fine sand was used to grout the bars and strands for Specimens J-P-Z4 through P-P-Z4.

The concrete and grout strengths are given in Table 2.

Test procedure

The boundary conditions and basic loading history for Specimens I-P-Z4 through K-P-Z4 are shown in Fig. 5. The load history was based on multiples of Δ_y, the measured yield displacement. Boundary conditions for the test specimens were as follows: pinned at the column bottom and roller supported at the column top and beam ends. Slight deviations from this basic load history were used in the actual tests; a third cycle at a particular displacement ductility was added if a significant loss in the peak lateral load occurred in the second cycle. Failure was considered to have occurred when the lateral load during a cycle dropped below 80 percent of the maximum load that was achieved in the first cycle at 2 Δ_y.

The load history used for Specimen L-P-Z4 (Fig. 6) was based on story drift and is the one used in the PREcast Seismic Structural Systems (PRESSS) Program (Priestley 1992). The change in the loading history was made from that used in Phases I through III so that comparisons with other PRESSS specimens could be made more easily. The following drift levels were used: 0.001, 0.0015, 0.002, 0.0025, 0.0035, 0.005, 0.0075, 0.01, 0.015, 0.02, 0.025, 0.03, 0.035, 0.04. Three cycles were completed at each drift level, followed by an intermediate elastic cycle. In the elastic cycle, the specimen was loaded to approximately 30 percent of the peak load in the preceding three cycles. Failure in this case was defined as the drift at which the lateral load falls below 80 percent of the maximum measured lateral load.

The testing of Specimens L-P-Z4 A and B was stopped at a drift level of 0.015 to prevent significant damage to the
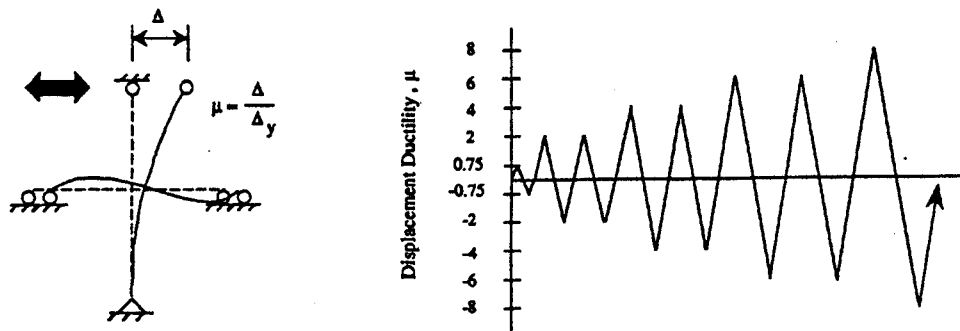
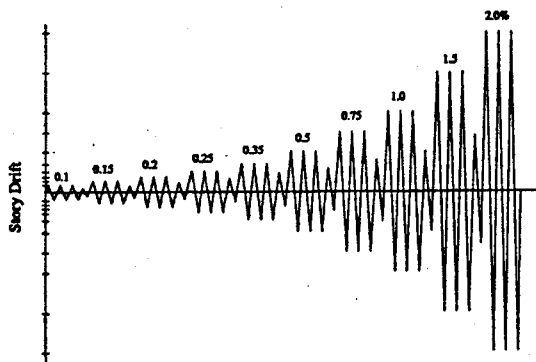Fig. 5—Boundary conditions and loading history

Fig. 6—Drift-based load history for Specimens L-P-Z4 to P-P-Z4

specimens, since some components were needed for subsequent testing.

All columns were subjected to an axial load approximately equal to $0.4 f_c' A_g$. The axial load was specified in the design provided by the precast contractor. Concentrated loads simulating gravity loads on the beams were applied to all the specimens. A concentrated load of approximately 20 kN (4.5 kips) was applied to each beam at approximately 89 mm (3.5 in.) from the column face. The load was equivalent to a uniform dead load of 5.3 kPa (110 psf) and live load of 2.4 kPa (50 psf). The loads on the beams were maintained constant throughout the tests.

Strain measurements in the beam longitudinal steel and ties were recorded. Also, the opening between the beam and column at the interface and slip of the beam relative to the column were monitored. Rotations of the beams were also measured. Monitoring of the loads with load cells in the PT bars in Specimen J-P-Z4 was possible as these bars were unbonded. In addition, displacements and loads at the top of the column, loads at the ends of the beams, and the applied beam loads were recorded.

Test results
Failure mode
a. Fully bonded mild and PT steels (I-P-Z4 and K-P-Z4): Specimen I-P-Z4 failed prematurely at a story drift of approximately 2.7 percent due to bond failure of the mild steel. The bond failure occurred only in the dogbone part of the beams and occurred at approximately 1.7 percent story drift.

The development length provided [305 mm (12 in.)] was considered to be adequate to fully develop the No. 3 bars in

accordance with UBC 2612 (c) and (d) (ICBO 1988). However, the bars were bonded by grouting into a rough duct rather than by being cast into concrete, as assumed in UBC, so strain gages were attached to obtain the strain profile along the bars. Failure of the specimen was attributed to the presence of the strain gages and their coatings on the mild steel, which eliminated approximately 40 percent of the available bond length and divided the remaining bond length into several short sections. This reduction in bond strength was confirmed by subsequent pullout tests with identical ducts, grout, and mild steel bars. As a result, the mild steel bars in the other Phase IV specimens were not instrumented.

Specimen I-P-Z4 failed at 2.7 percent story drift. The specimen was not severely cracked, but the beam corners at the column face crushed. Due to the lack of significant damage to the column, the column was salvaged and used in Specimen K-P-Z4. New beams were constructed.

Specimen K-P-Z4 failed due to fracture of the mild steel. Fig. 7 shows Specimen K-P-Z4 at failure at a story drift of 3.1 percent. This failure mode differed from that for the monolithic Zone 4 specimens, which was plastic hinging of the beams with no bar fracture. This is likely a result of greater mild steel strains in the precast specimen due to concentration of the beam rotation at the column face, whereas the beam rotation in the monolithic specimen was distributed over the plastic hinge length.

This specimen, like the previous ones, experienced extensive concrete crushing at the beam corners adjacent to the joint. Crushing of the beam corners first occurred at a drift level of approximately 0.9 percent. The shape of the hysteresis curves (to be seen in Fig. 12) indicates that the mild steel bars were close to yield or began to yield at this drift level. At a story drift of approximately 2.0 percent, the concrete in the column around the mild steel bars began to form a "cone" and to pull out. Significant spalling of the column concrete also occurred around the mild steel bars. The width of the joint opening at failure (3.1 percent story drift) was approximately 11 mm (0.43 in.). At the end of the test, no vertical slip of the beams or bond failure of the mild steel was observed. Also, the beam crack widths were less than 1 mm (0.04 in.).

b. Bonded mild steel and unbonded PT steel [J-P-Z4]: Failure of Specimen J-P-Z4 was caused by fracture of the mild steel bars. Fig. 8 shows the specimen at failure at a story drift of 3.6 percent. A total of six bars fractured; the first and second fractured at 3 percent story drift and the other four at
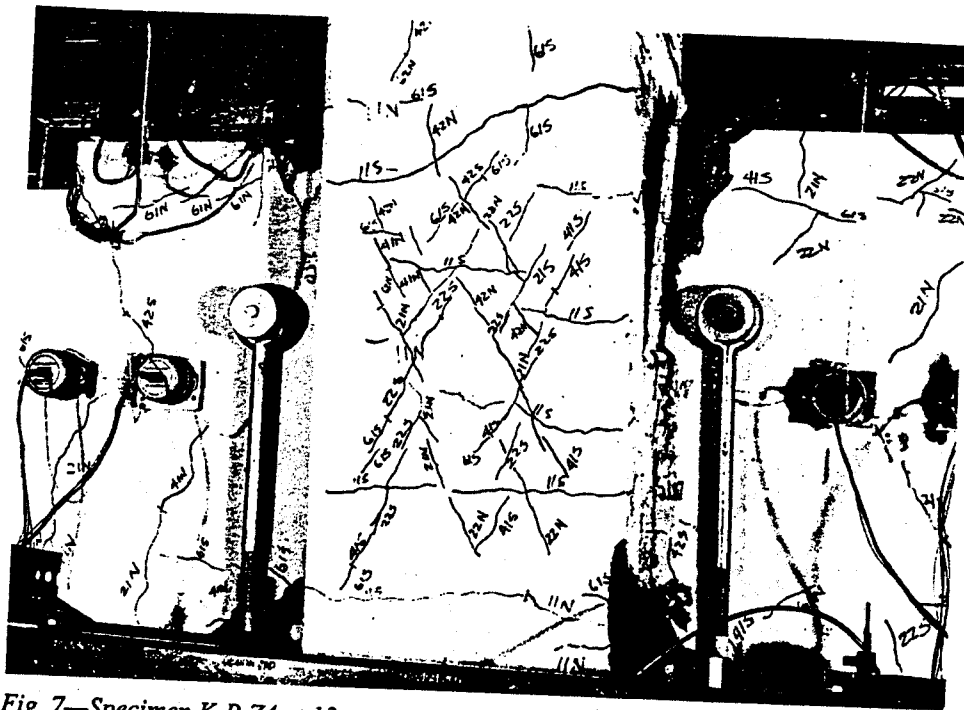
234

Fig. 7—Specimen K-P-Z4 at 13 percent story drift, failure

Fig. 8—Specimen J-P-Z4 at 3.6 percent story drift, failure

a story drift of 3.6 percent. Load cell readings indicated that one of the PT bars yielded at approximately 1.7 percent drift, while the loads in the remaining PT bars were slightly less than the yield load. These PT bars did not yield at later stages in the test. Yielding of the PT steel was likely caused by its proximity to the extreme fiber and by its lower yield strength of 896 MPa (130 ksi), as compared to the yield strength of approximately 1738 MPa (252 ksi) for the strands.

Crushing of the beams at the corners initiated at approximately 1.0 percent story drift. The corners of the beams in Specimen J-P-Z4 were protected by steel angles and so did not experience as much spalling as those in Specimen K-P-Z4. Pullout of the concrete in the column around the mild

steel bars began at about 2.0 percent story drift; there was no corresponding pullout cone in the beam, again due to the presence of the angles. At the conclusion of the test, these regions in the column had significant spalling.

The shape of the hysteresis curves (to be shown in Fig. 11) indicates that the mild steel bars yielded at approximately 1 percent story drift. Readings from the load cells indicated that one of the PT bars yielded at 1.7 percent story drift and that, while the other three PT bars were close to yielding, they did not yield at this drift level nor at a higher drift level.

The beams in Specimen J-P-Z4 sustained more extensive shear cracking than did those of Specimens I-P-Z4 and K-P-Z4. Several points are worth noting when comparing the
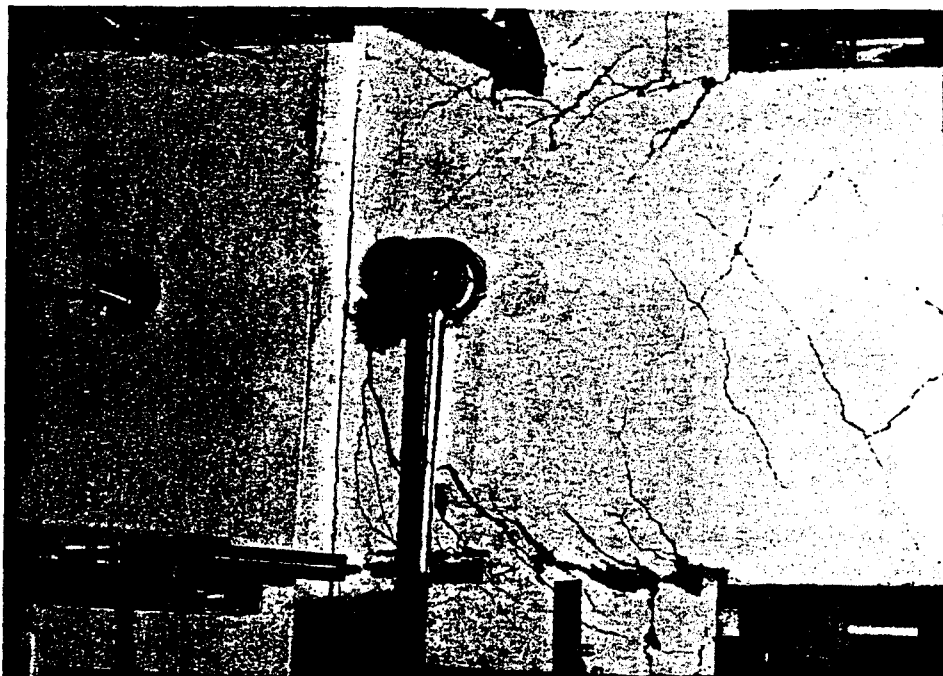
Fig. 9—Specimen L-P-Z4 at failure, 20 percent

specimen behaviors. First, the absence of PT in the main part of the beam of J-P-Z4 lowered its total shear resistance and the load at which shear cracking started. The other two specimens contained PT in the beam.

Second, the area of shear reinforcement for Specimen J-P-Z4 was 20 percent less than for Specimens I-P-Z4 and K-P-Z4. This was unintentional and was a result of the specimens being designed by different agencies.

Third, the shear reinforcement was designed in accordance with UBC seismic provisions (ICBO 1988), which are based on the largest shear force that could occur given the beam flexural strengths at its ends. The real stress in the mild steel flexural reinforcement at incipient fracture was higher than the 1.25 f_y anticipated by UBC, but the stress in the PT was lower than this value. The net result was that the real shear force was slightly higher than that allowed for in design.

Fourth, the shear strength was just sufficient, but the shear cracks were wide enough [about 2 mm (0.08 in.)] to have required extensive repair, had this been a real structure. One possible advantage for the precast system, which would render it superior to a comparable monolithic system, is to concentrate the damage in the connection steel and thereby avoid potential costs of concrete repair. Thus, there is a case for designing shear reinforcement not only for strength but also for crack control.

Finally, the specimen ties were made from smooth wire, which derives its anchorage largely from the bends around the main bars. Therefore, the vertical legs probably slipped more than their prototypical counterparts, and the specimen crack widths were probably greater than those to be expected in the field. This is true of the shear cracks in all of the model specimens.

c. Unbonded mild and PT steels (replaceable system) (L-P-Z4, A, B, and C): Specimens L-P-Z4 A and B were not tested to failure. These specimens contained PT steel at the top and bottom of the beams but no mild steel. The purpose

was to determine which type of PT steel would behave best before testing the joint in its intended configuration of combined mild and PT steel. Both specimens sustained fine shear cracks in the beams and very minimal crushing of the beam at the column face through a story drift of 1.5 percent. However, at a drift of 1.5 percent, the PT bars yielded in Specimen L-P-Z4 B. The column in both tests experienced no damage other than a few very minor cracks. At the end of the test, the strands in Specimen L-P-Z4 A had lost approximately 30 percent of their initial force, while the PT bars in Specimen L-P-Z4 B lost approximately 80 percent of their initial force. The latter is attributed to bar yielding, but the loss of strand prestress was more likely caused by seating at the chucks and by local crushing of the grout and beam concrete. The strand load cells showed that the strand stress reached 1259 MPa (183 ksi). This was higher than the jacking stress (so seating is plausible) but lower than the yield stress. The 30 percent force loss corresponds to a total change in length of only 1 mm (0.04 in.). In a full-scale prototype, the change in length would still be the same, so the changes in strain, stress, and force would be significantly smaller.

Failure of Specimen L-P-Z4 C resulted from shear cracks that formed at the interface between the flange of the T-section and the beam in the dogbone region, as seen in Fig. 9. Despite the bars welded to the T-section and the heavy shear reinforcement, significant slip occurred along the failure plane before the required resistance developed. The shear cracks, approximately 3 mm (0.12 in.) in width, turned vertical at the column face and formed a sideways U-shaped failure plane. The specimen failed at 2 percent story drift. At this point, the vertical cracks were approximately 5 mm (0.20 in.) wide. This undesirable mode of failure would likely not occur if a reinforcing cage were used instead of the T-section.

The mild steel tubes in Specimen L-P-Z4 C yielded at approximately 0.75 percent story drift. Beam crushing and spalling occurred at a story drift of 1.5 percent. Splitting

236

Table 3—Connection strength and story drift

Specimen	Moment, kN-m		Experimental story drift at failure, percent	No. of loading cycles to failure
	Predicted	Measured		
A-M-Z4, B-M-Z4	132	148/153	3.7/3.4	8/8
I-P-Z4*	133†	138	2.7	7
J-P-Z4	153†	152	3.6	12
K-P-Z4	139†	151	3.1	7
L-P-Z4 A‡	126†	105	1.5	36
L-P-Z4 B‡	98†	82	1.5	36
L-P-Z4C§	141†	117	2.0	38

*Bond failure of mild steel.
†Moments obtained from analysis program which calculates moments for a section given an imposed beam rotation; these moments are the maximum moments calculated.
‡These specimens were not tested to failure.
§Shear failure in beam.
1 kN-m = 0.738 k-ft

cracks also formed at the bottom of the dogbones at this drift level. The maximum forces in the PT strands ranged from $0.65 f_{py}$ to $0.75 f_{py}$. Throughout the three tests, the column sustained minimal damage.

Due to the extent of the shear cracks observed in the beams of Specimen J-P-Z4, the transverse reinforcement in Specimen L-P-Z4 was doubled. However, this increase in the amount of transverse reinforcement did not significantly reduce the amount of shear cracks in Specimen L-P-Z4. This is not surprising because, although the increased steel resulted in increased strength, the concrete must still crack before the steel strains can reach yield.

Comparison of the performance of Specimen K-P-Z4 (central PT) with that of Specimen J-P-Z4 and L-P-Z4 (PT top and bottom in dogbone) indicates that post-tensioning the entire beam is more effective than increasing the transverse reinforcement in reducing shear cracking in the beams. This is because the precompression requires a greater force to crack to the concrete.

Story drift—The story drifts at failure are given in Table 3. A comparison of Specimens J-P-Z4 and K-P-Z4 shows that Specimen J-P-Z4 achieved a slightly higher drift level at failure.

The hysteresis plots for the specimens are given in Fig. 10 through 13. Specimen J-P-Z4 (Fig. 11) underwent smaller increases of story drifts than did Specimen K-P-Z4 at each new load level. The load history was based on multiples of Δ_y. However, in Specimen J-P-Z4, strain compatibility was incorrectly assumed when calculating the maximum moment. The result was that M_{max} and Δ_y were calculated incorrectly. The use of drift-based loading histories adopted for the Phase IV-B tests reduces the sensitivity of the test procedure to the analytical modeling techniques.

Connection strength—The maximum measured moments for all the precast specimens exceeded the predicted values. Except for the two cases where the failure mode was unanticipated (I-P-Z4 and L-P-Z4 C), the measured flexural strength of the precast specimens matched that of the monolithic specimens. The moments in Table 3 for the monolithic specimens were calculated based on the actual yield stress of the steel with a factor of 1.25 applied to it to account for steel strain hardening, the 28-day concrete compressive strength, and an ultimate concrete strain of 0.003.

As seen in Table 3, the experimental moments obtained for the monolithic specimens were on average 14 percent greater than the calculated moments. For the precast specimens, excluding Specimens L-P-Z4 A-C, which failed prematurely, the experimental moments were on average 5 percent higher than the calculated moments.

Energy dissipation—Due to the different yield displacements and concrete strengths for the specimens, it was felt that the most practical means to compare the energy dissipation was to plot the dimensionless cyclic energy dissipated against the story drift. The dimensionless quantity of cyclic energy dissipated was determined by dividing the energy dissipated per cycle by four times the product of the maximum experimental load and the maximum displacement for that cycle. The denominator is multiplied by four because this will then yield a rectangular perfectly elasto-plastic loop, and the values on the ordinate axis represent, as a ratio, the energy dissipated for that cycle to the elasto-plastic loop. In Fig. 14, the normalized cyclic energy was plotted against the story drift, and a best-fit curve was drawn through these points.

Specimens J-P-Z4, K-P-Z4, and L-P-Z4 C matched the energy dissipation of the monolithic specimen up to approximately 1.5 percent story drift. Specimen K-P-Z4, with PT steel in the center and mild steel top and bottom of the beam, and Specimen J-P-Z4, with PT steel and one-third more mild steel at the beam top and bottom, had similar cyclic energy dissipation. After fracture of the mild steel, the drop in cyclic energy dissipation was greater for Specimen J-P-Z4 than for Specimen K-P-Z4. This greater drop was likely due to the larger loss of prestress in Specimen J-P-Z4 as a result of the PT steel yielding. After fracture of the mild steel bars in Specimen K-P-Z4, the normalized cyclic energy dissipation curve was similar to those of the other precast specimens with PT steel only (Cheok and Stone 1993). The implications of this behavior are that even if seismic-induced strains exceed the fracture strain for the energy-dissipative steel, a fail-safe residual strength level will be provided by the PT steel, albeit with less damping.

General discussion

The tests showed that a precast concrete system based on hybrid reinforcement is feasible and shows considerable promise. Not all of the details worked perfectly, but the pur-
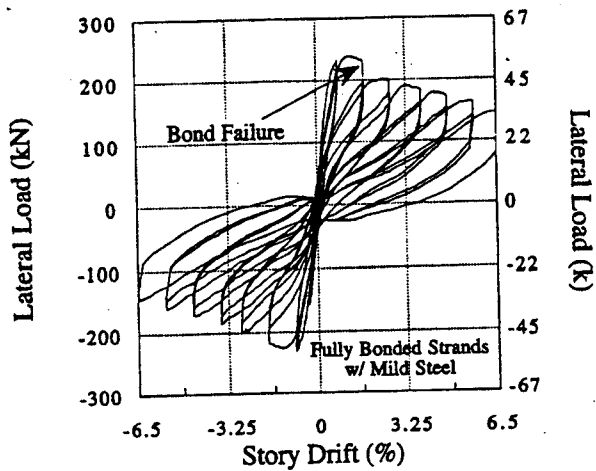
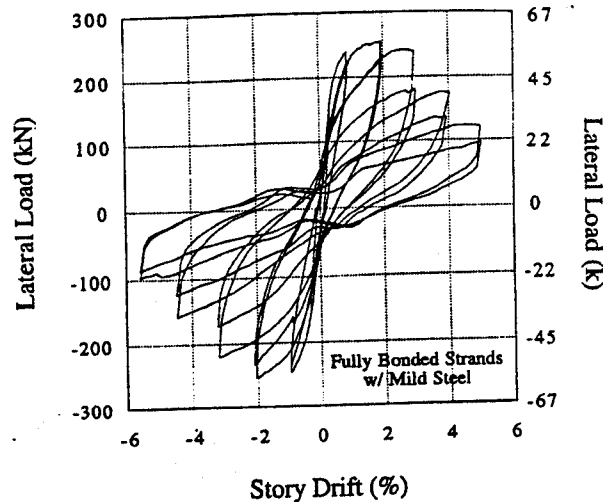Fig. 10—Hysteresis curves for I-P-Z4

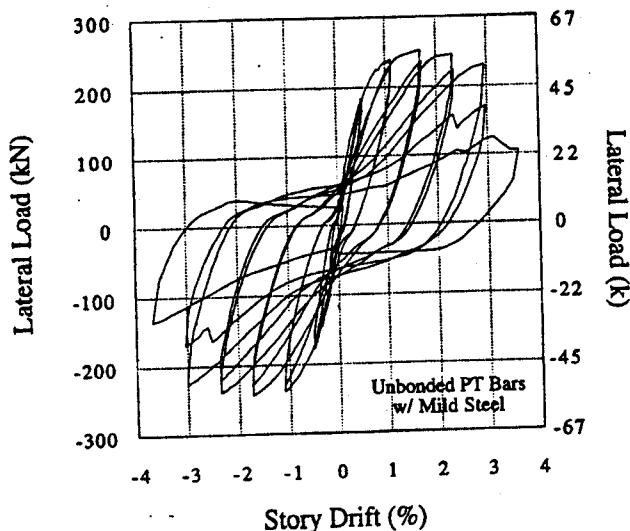Fig. 12—Hysteresis curves for K-P-Z4
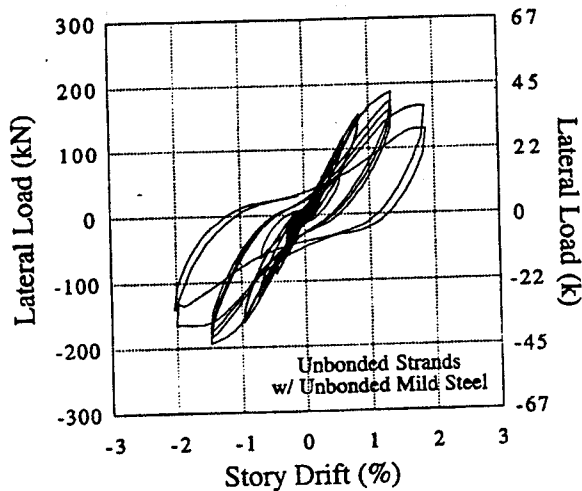

Fig. 11—Hysteresis curves for J-P-Z4

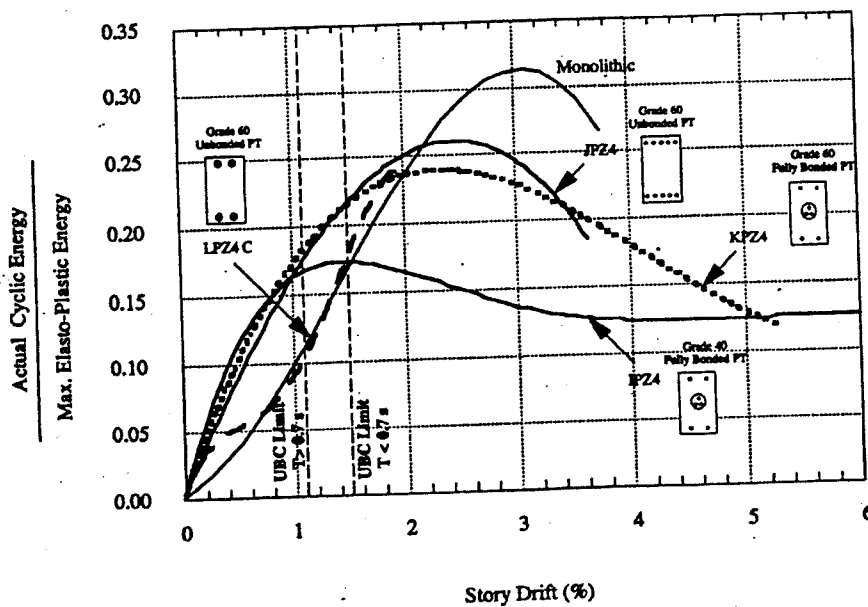Fig. 13—Hysteresis curves for L-P-Z4 C

Fig. 14—Comparison of normalized cyclic energy and story drift

pose of the program was to evaluate a number of concepts and to identify the most promising one. The key issues are that, given the appropriate details, the PT steel remains elastic and the system loses little strength up to very large drifts, the mild steel dissipates energy, and no shear slip occurs at the beam-column interface. Based on these issues, Specimen K-P-Z4 showed the most promise.

The drift at which the PT steel yields is influenced by the PT location, the type of steel, and the initial prestressing stress. Strands prove better than bars because their yield strains are higher. The PT is best located at middepth of the beam, which minimizes the increase in strain for a given rotation or drift. The lowest initial prestressing stress consistent with other constraints should be used because the greatest strain capacity remains to accommodate drift. The need for shear friction resistance places a lower bound on the prestress force than can be used, so very low stress could lead to large and uneconomical tendons. Even if the PT steel yields, its contribution to the flexural strength is not lost, but rather the danger is one of possible shear slip at the column face. This behavior represents a fail-safe feature. It should also be noted that at the reported failure drift, the systems still maintained 80 percent of their maximum strength. In some cases, the damage at failure was small compared to that in a conventional reinforced concrete joint.

Obtaining successful behavior in the mild steel depends on the detailing. Bond must be assured for anchorage, and any unbonded length must be great enough to prevent fracture (as in K-P-Z4), but short enough to insure that yielding takes place. The mechanical connections of the replaceable system (L-P-Z4) lead to relatively large unbonded length, and yielding was further inhibited by the relatively high yield strength of the steel. The mechanical connectors performed as intended but they added material cost, caused congestion, and were time-consuming to assemble both during fabrication and erection. The specimens with the bars grouted in the ducts (I, J, and K P-Z4) provided energy dissipation that was equal to or larger than that of the monolithic specimens up to about 1.5 percent drift.

Slip was prevented at the beam-column interface because the fiber reinforced grout maintained its integrity, and the PT strand remained elastic.

The tests also demonstrated that the systems with central PT provided significantly better structural performance. The body of the beam suffered almost no shear cracking when central PT was present and serious cracking when it was not. A simple truss model shows why—in the absence of gravity shears and mild steel, the seismic shear is carried by a single compression strut and, theoretically, no ties are needed at all. The problem of shear transfer into the dogbones is acute and, even with large quantities of shear steel, cracking and slip occur well before failure. The reinforcing is also congested and difficult to install. Lastly, the dogbones are an architectural inconvenience.

The preceding considerations suggested that a successful design should contain central PT, grouted mild steel at top and bottom, and no dogbones. Fig. 15 shows a possible design. The solid beam end-houses the ducts for the mild steel, and the trough allows the bars to be lowered into place and slid into the ducts. The troughs can be filled later if desired.
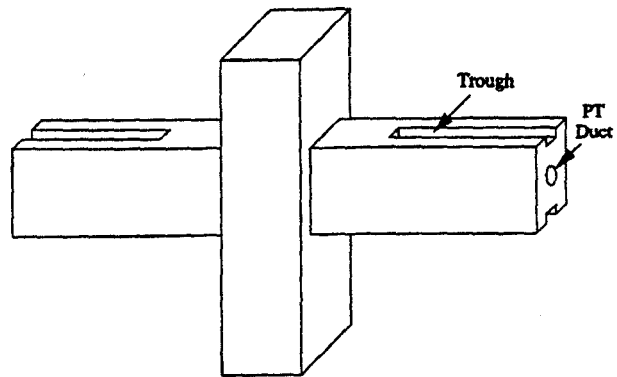

Fig. 15—Trough beam used in Phase IV-B specimens

The connection between the beam bars and the bars in the ducts is now a "beam" that spans horizontally across the width of the real beam, rather than cantilevering up and down as was the case in the dogbone designs. This design was used for subsequent tests.

Conclusions

The following conclusions can be drawn from the study:

1. The use of both unbonded PT and bonded mild steel for connecting precast concrete beams and columns is feasible. The PT steel clamps the beam against the column to provide shear resistance, while the mild steel dissipates energy through cyclic yielding.

2. The best PT arrangement is to use strands, placed at middepth of the beam, running over the full length of the building. They should be stressed less highly than in conventional PT construction.

3. The mild steel experiences high local strains at the beam-column interface. These could lead to premature fracture if they are not alleviated. Debonding a short length on either side of the interface is a potential solution.

4. The amount of energy dissipated by the specimens containing bonded mild steel was equal to or greater than that in the conventionally reinforced system up to approximately 1.5 percent drift.

5. A more detailed study, which uses the details that were identified here as being the best, was necessary to find the most suitable values of parameters such as prestressing stress. Such a study is reported in Cheok and Stone (1994).

PHASE IV-B SPECIMENS

Introduction

Four beam-column connections were tested in Phase IV-B. The precast beams and columns were fabricated by a precaster and were shipped to NIST where they were assembled and tested. The objective was to determine the optimum combination of mild and PT steels and to examine the use of an alternate type of mild steel as a means of improving the energy-dissipation characteristics of the connection.

The design forces used were the same as those used in Phase IV-A. However, since one of the variables in the Phase IV-B specimens was the amount of mild steel, the maximum moment capacities served as an upper bound in the design of the beams.
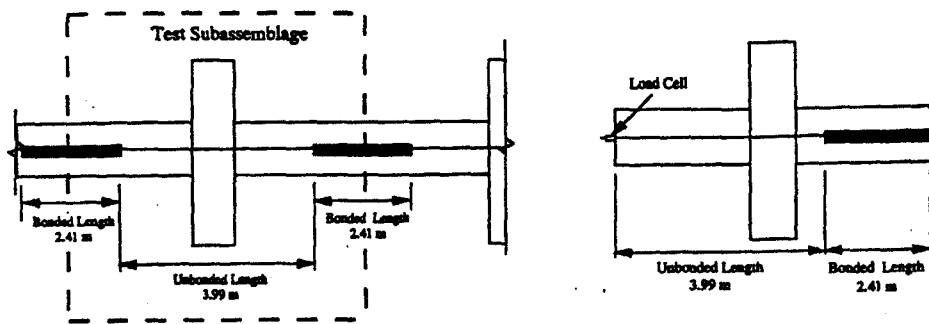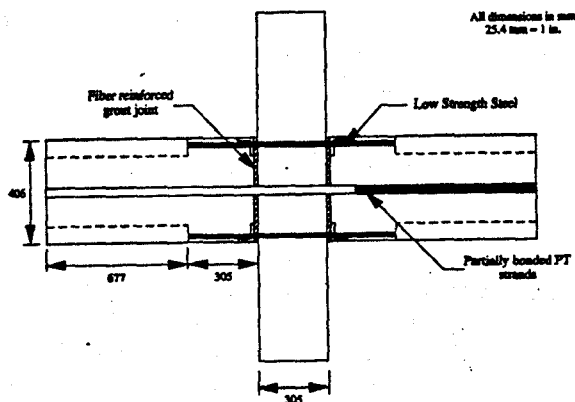
Fig. 16—Bonding of PT steel

Fig. 17—Basic details for Specimens M-P-Z4 to P-P-Z4

The results of the Phase IV-A tests provided guidance on the relative amounts of mild and PT steel to be used, but the choices were limited by the bar sizes available. The final decision was to use either two No. 3 bars or three No. 3 bars, made of either A 615 steel or ASTM A240-87 304 stainless steel, and three 13-mm ($^1/_2$-in.) Grade 270 strands. Thus, four specimens were tested in all, and the ratios of the moment contributed by the mild steel to the total moment were approximately 35 and 47.

The reason for using 304 stainless steel bars as the energy dissipators was that 304 stainless steel has a total strain elongation capacity of approximately 50 percent compared to about 20 percent for the Grade 60 reinforcing bars. The greater elongation capacity was expected to provide better energy dissipation and to delay fracture.

The Phase IV-A tests demonstrated the structural advantages of using unbonded PT tendons. However, a fully unbonded design runs the risk of complete loss of prestress along one side of the building should an end anchorage fail. Therefore, it was decided that the tendons would be unbonded through the column and for a distance on either side of the column and would be bonded at midspan of each bay, as shown in Fig. 16(a). The length of the unbonded distance in the beam depends on the required development length for the tendons. This arrangement addresses the concern for progressive collapse for an unbonded PT system.

Monitoring the loads in the PT steel throughout the tests was considered desirable. The use of strain gages was rejected for practical reasons. So the PT steel was grouted as

shown in Fig. 16(b), and load cells were installed on each tendon on the unbonded side. The total unbonded length of the tendon was the same as it would have been if it had been located centrally, so the performance was expected to be unaffected by the asymmetry.

Steel angles were also included at the corners of the beams at the column interface as it was shown that the beams in J-P-Z4 suffered less damage in these regions than did those in Specimens I-P-Z4 and K-P-Z4, which did not utilize reinforcing angles. Prevention of concrete crushing at the beam corners is especially necessary at higher drift levels.

In summary, the Phase IV-B connections were post-tensioned centrally with the strands partially bonded. Steel angles were included at the corners of the beams at the column face. Two types of mild steel were used for the reinforcing bars: A 615 Grade 60 ($f_{py} = 414$ MPa) and A 240 Type 304 stainless steel ($f_{py} = 414$ MPa).

Specimen details

The configuration of Specimens M-P-Z4 through P-P-Z4 was the same and is shown in Fig. 17. The specimens were post-tensioned with three 13-mm ($^1/_2$-in.) Grade 270 ($f_{pu} = 1862$ MPa) prestressing strands [ASTM A 416-87a (ASTM 1988)] located at the beam centroid and stressed to $0.44 f_{pu}$.

The specimens varied only in the amount and type of mild steel they contained. The mild steel in Specimens M-P-Z4 and O-P-Z4 consisted of two No. 3 (top and bottom) and three No. 3 (top and bottom) reinforcing bars, respectively. The mild steel in Specimens N-P-Z4 and P-P-Z4 consisted of two 9-mm (0.36-in.) and three 9-mm (0.36-in.) 304 stainless steel bars, respectively. The main reinforcement details for the specimens are given in Table 4. The dimensions of the beam were 203 x 406 mm (8 x 16 in.).

The stainless steel bars were machined from 11-mm (7/16 in., N-P-Z4) and 13-mm ($^1/_2$-in., P-P-Z4) round stock with thread patterns shown in Fig. 18. The thread pattern shown in Fig. 18(b) provided better bond and was adopted after the mild steel bars debonded during the test of Specimen N-P-Z4.

The mild steel bars were intentionally debonded for 25 mm (1 in.) on both sides of the beam-column interface to delay bar fractures as observed in Phase IV-A. The debonded length was kept short to avoid bond failure. However, in addition to changing the deformation pattern, the stainless steel bars in Specimen P-P-Z4 were fully bonded to maximize the
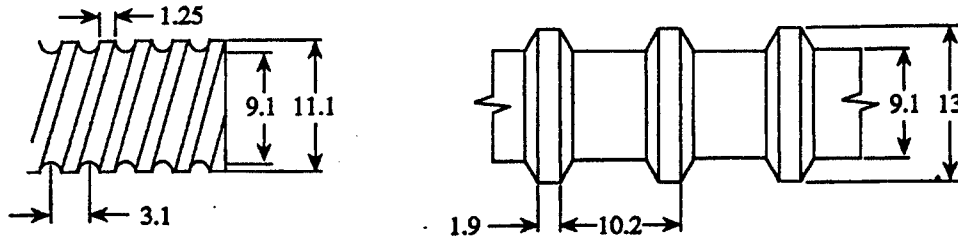
Fig. 18—Threads for stainless steel bars

bond length to prevent bond failure as occurred in the test of Specimen N-P-Z4.

Beam stirrups and column ties were welded reinforcement grids (WRGs) custom made for the specimens and were made from smooth wire. This avoided potential congestion of hooked bars and eliminated the need for tight radius bends.

The design concrete strength was 41.4 MPa (6000 psi). The reinforcing steel in beams and columns was A 615 Grade 60 (f_{py} = 414 MPa). The actual material properties are given in Table 2.

Post-tensioning and grouting procedures

When post-tensioning the specimens, the strands were pulled to 0.8 f_{pu} to seat the chucks. This lessened the load losses in the strands caused by seating of the chucks during the tests at high drift levels. The loads in the strands were then released and were restressed to approximately 0.7f_{pu}, at which point shims were placed under the chucks as necessary. The sizes of the shims then were adjusted so that the final stresses in the strands were approximately equal to 0.44 f_{pu}.

As with the specimens in Phase IV-A, the ducts used in the Phase IV-B specimens for the mild steel were made of 13-mm ($^1/_2$-in.) ID electrical conduit. These conduits were removed by unwinding after the beams were cast. This allowed greater clearance and easier grouting of the mild steel. A fine-sanded grout was used to grout the mild steel bars and the PT steel. The construction joint was made of a fiber reinforced grout. The strengths of grout used in the joints and in the ducts are given in Table 2.

Test procedure

The load history used for Specimens M-P-Z4 through P-P-Z4 was based on story drift and was similar to that used for Specimen L-P-Z4 (Fig. 6). The only difference was that the load history used for the Phase IV-B specimens began at a story drift level of 0.2 percent. In addition, after the completion of three cycles at 3 percent drift, P-P-Z4 was subjected to cycles beginning at 1 percent, 1.5 percent, etc. to simulate an aftershock. The imposed loads on the columns and beams simulating gravity loads were the same as in Phase IV-A. The instrumentation for displacement and rotation measurements in Phase IV-B was the same as that used in Phase IV-A. The location of the strain gages was changed in Phase IV-

B. In each beam, two WRGs, one located at the column face and the other at the transition from the rectangular cross section to the H section of the beam, were instrumented with two strain gages each.

Test results

Behavioral failure mode—In general, the crack widths in all the specimens, both beams and columns, were very small [<1 mm (0.04 in.)] throughout the tests, and these cracks closed at zero displacement. Because of this, the strains in the beam ties were very low and were approximately 10 to 15 percent of yield. Also, joints between the beam and column closed completely at zero displacement, even after story drifts of 3.0 to 3.5 percent, indicating the ability of the connection to re-center itself and prevent permanent drift.

As the PT steel was bonded in one beam and unbonded through the other, there existed a possibility that the crack pattern might differ in the two beams. However, no difference was observed.

In all specimens, crushing of the beams began at a story drift of 0.75 percent. The beam corners at the column face sustained some minor crushing at the ends of the angle leg on the beam face inside the angle. Significant crushing of the grout joint occurred in the later stages of the tests, but the grout was held together by the fibers. As with the Phase IV-A specimens, no vertical slip of the beam relative to the column was observed during the tests.

Table 4 summarizes the specimen performance. Fig. 19 through 24 show photographs of the monolithic and hybrid specimens at critical events, and Fig. 25 and 26 show the variation in PT force throughout the tests. Description of the individual tests follow.

a. Specimen M-P-Z4 (two No. 3, Grade 60 reinforcing bars, top and bottom): Fracture of mild steel bars caused the failure of Specimen M-P-Z4. Fig. 20 shows the connection at failure (3.4 percent story drift). The maximum opening between the beam and column at failure was 13 mm ($^1/_2$-in.). For purposes of comparison, Fig. 19 shows a monolithic connection at failure. The difference in shear cracking both in the beams and column is evident.

The force in a typical strand is shown in Fig. 25. The peak stresses and stresses at the end of each test are given in Table 4. For M-P-Z4, the peak average stress in the PT steel was 0.85 f_{pu}, which indicates that it remained in the elastic range throughout the test (f_{py} = 0.93 f_{pu}). There was only a minimal

Table 4—Phase IV-B specimen details

Specimen	Monolithic*	M-P-Z4	N-P-Z4	O-P-Z4	P-P-Z4
PT steel	—	3-13 mm	3-13 mm	3-13 mm	3-13 mm
Initial bm prestress, MPa	—	2.98	2.83	2.76	3.00
Mild steel	5-#3, 2-#4	2-#3, Grade 60	2-9 mm, SS†	3-#3, Grade 60	3-9 mm, SS†
f_y, MPa	414	414	414	414	414
$M_{pred,max}$ kN-m	132	109	116	126	124
$M_{non\,pt}/M_{tot}$	1.0	0.35	0.36	0.45	0.47
Load history	Multiple of Δ_y	0.2 to 3.5%	0.2 to 3.5%, 6%	0.2 to 4.0%	0.2 to 3%, 1 to 3%
Cycles to failure	8	42	38	43	57
Drift at failure, percent	3.6	3.4	2.9	3.4	>3.0
Maximum drift, percent	3.6	3.5	6.0	4.0	3.5
Drift at peak stress, percent	—	3.4	5.9	3.9	3.4
M_{exp}, kN-m	151	119	116	139	128
M_{exp}/M_{pred}	1.14	1.09	1.00	1.10	1.03
Failure	Plastic hinging	Bar fracture	Debonding	Bar fracture	Bar fracture
Strands:					
Initial stress	—	$0.45 f_{pu}$	$0.42 f_{pu}$	$0.41 f_{pu}$	$0.45 f_{pu}$
Average peak stress	—	$0.85 f_{pu}$	$0.94 f_{pu}$	$0.88 f_{pu}$	$0.84 f_{pu}$
Average stress at end of test	—	$0.38 f_{pu}$	$0.11 f_{pu}$	$0.39 f_{pu}$	$0.52 f_{pu}$

*Values are average of two monolithic tests.
†Stainless steel bars.
1 kN-m = 0.738 kip-ft; 1 MPa = 0.145 ksi; 25.4 mm = 1 in.

loss in the initial prestress due to crushing of the grout, beam concrete, etc. The clamping force required to resist the gravity loads was maintained throughout the test to failure.

b. Specimen N-P-Z4 [two 9-mm (0.36-in.) ASTM 240 Type 304 stainless steel bars, top and bottom]: Specimen N-P-Z4 failed prematurely due to bond failure of the stainless steel bars. In each case, the bond in only one beam and in the column failed. Bond failure of the first bar occurred at approximately 2 percent story drift. Bond failure occurred at approximately 2.5, 3, and 6 percent (second cycle) for the remaining stainless steel bars. The bar which debonded at 6 percent story drift had yielded in the first cycle at 6 percent before debonding. The opening between the beam and column at 6 percent story drift was 23 mm (0.91 in.). Fig. 21 and 22 show the specimen at story drifts of 2.9 percent (nominal failure) and 5.9 percent.

Due to the debonding of the mild steel, a decision was made to cycle the specimen to 6.0 percent story drift after the cycles at 3.5 percent story drift. This was because no yielding of the stainless steel bars was expected to occur due to the debonding and, therefore, little additional information on the energy-dissipation characteristics could be gained by cycling the specimen at story drifts of 4.0 percent, 4.5 percent, etc. The specimen was cycled at 6.0 percent story drift to determine the stress in the PT steel and the ability of the connection to resist both the applied and gravity loads at this drift level.

Table 4 shows (and Fig. 28 will show) that the PT steel yielded at a story drift of 5.9 percent, which eliminated 75 percent of the prestress force. However, sufficient clamping force was still produced by the PT steel to resist the gravity loads, as no vertical slip of the beam relative to the column

was noted at zero displacement. As shown in Fig. 26, the strands did not yield at 3.5 percent story drift.

Deformed stainless reinforcing bars were not available, so they were fabricated by machining smooth bars as mentioned earlier. However, these bars suffered bond failure before they yielded. The profile of the deformations was redesigned [Fig. 18(b)], based on preliminary findings reported by Darwin (Darwin and Graham 1993), and the bond for P-P-Z4 proved adequate. Because the length available for bonding was limited, further investigation of the development length for grouted bars under cyclic loading is warranted.

Specimen O-P-Z4 (three No. 3, Grade 60, reinforcing bar, top and bottom): Failure of the specimen resulted from fracture of the mild steel bars. Bar fracture occurred at story drifts of approximately 3.5 and 4.0 percent. Eight bars (six bars/joint) fractured in this specimen. The opening between the beam and column at failure was 11 mm (0.43 in.). Fig. 23 shows the specimen at failure and a story drift of 3.4 percent.

The PT steel remained in the elastic range through failure with an average peak stress of $0.88 f_{pu}$. The total loss in prestress in the PT steel was $0.02 f_{pu}$. The forces in the PT strands were similar to those for M-P-Z4 (Fig. 25).

d. Specimen P-P-Z4 [three 9-mm (0.36-in.) 304 stainless steel bars, top and bottom]: Two tests were conducted on Specimen P-P-Z4. In the first, the load history of Fig. 6 was followed up to 3 percent drift, and no damage to the steel was observed. As Fig. 14 shows, the monolithic connection exhibited maximum cyclic energy dissipated at approximately 3 percent. Since Specimen P-P-Z4 did not show any signs of strength degradation, it was decided to study the performance of the specimen if it were to be subjected to an aftershock. Therefore, the load sequence was restarted at 1

Fig. 19—Monolithic specimen, A-M-Z4, at failure (3.7 percent story drift)
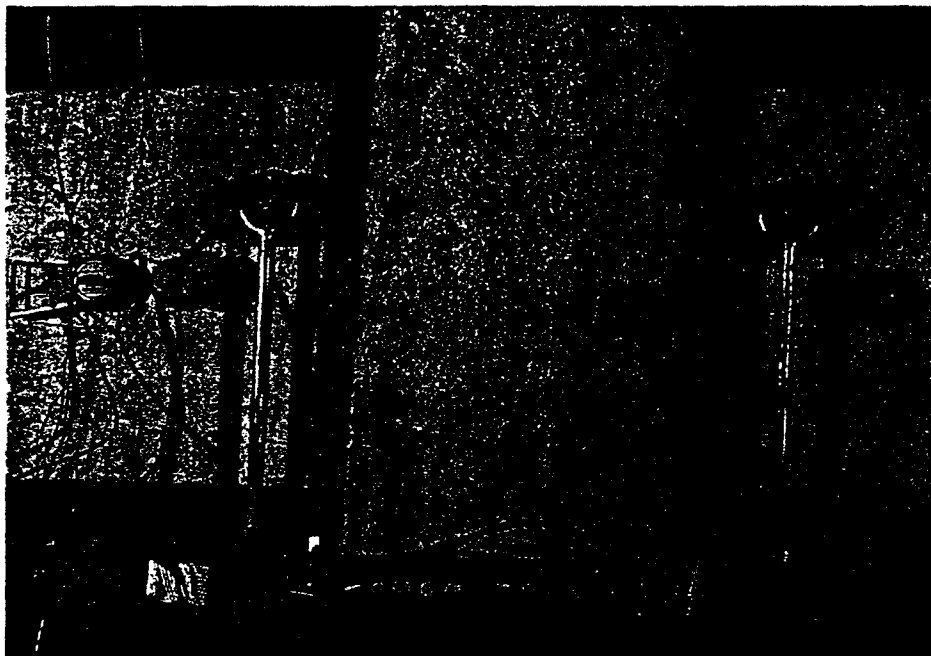

Fig. 20—M-P-Z4 at failure (3.4 percent story drift)

percent drift and continued until bars fractured between 2 and 3 percent drift. Nominal failure occurred at 2.9 percent drift. Fig. 24 shows Specimen P-P-Z4 at failure.

At the end of the test, the PT force closed the cracks; no concrete damage, apart from minor spalling at the angles, was visible. Similar behavior was observed in all the tests.

The stainless steel bars probably fractured through low-cycle fatigue. They experienced a total of 57 cycles of load and a cumulative extension of approximately 185 mm (7.28 in.). This is equivalent to several severe earthquakes.

A large area of concrete cover pulled out of the column around the mild steel bars and spalled off. Similar but less extensive spalling occurred in the other specimens. This difference may have been caused by the fact that the mild steel

bars in this specimen were fully grouted, whereas the bars in the other specimens were debonded 25 mm (1 in.) on either side of the beam-column interface. The different lug pattern may also have been partly responsible.

The forces in the prestressing strands for P-P-Z4 were similar to those for M-P-Z4. As with the previous Phase IV-B specimens, the PT steel remained elastic with an average peak stress of $0.84 f_{pu}$ up to 3.5 percent drift. As seen in Table 4, the stress in the PT steel at the end of the test, $0.52 f_{pu}$, was greater than the initial stress, $0.45 f_{pu}$.

Two possible reasons are offered for this increase in stress. At the end of the test, a gap of approximately 0.8 to 1.6 mm (0.03 to 0.06 in.) existed between one of the beams and the column. This gap corresponded to an increase in stress in the
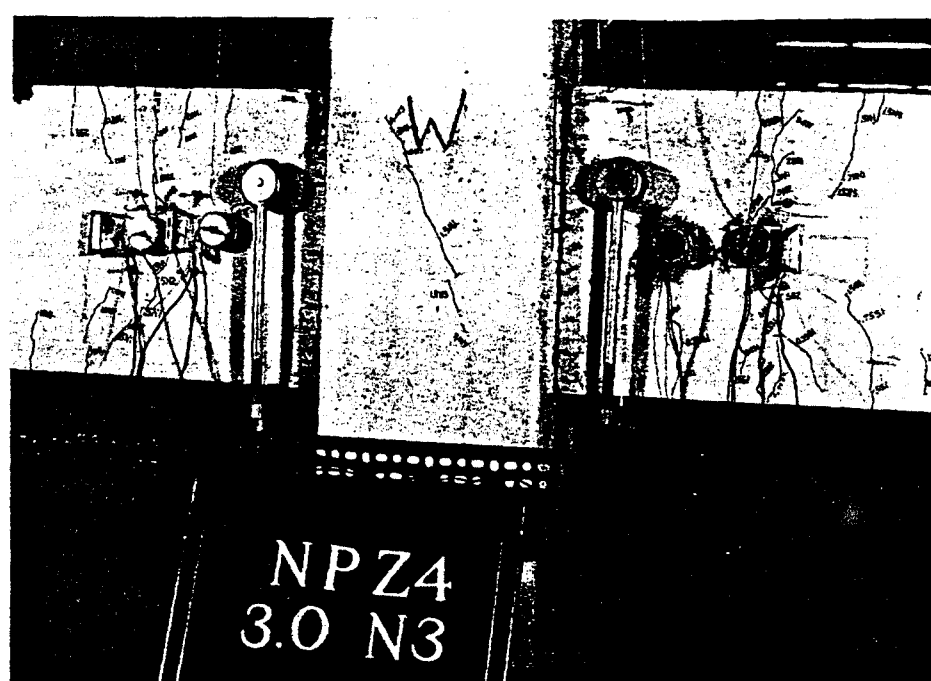
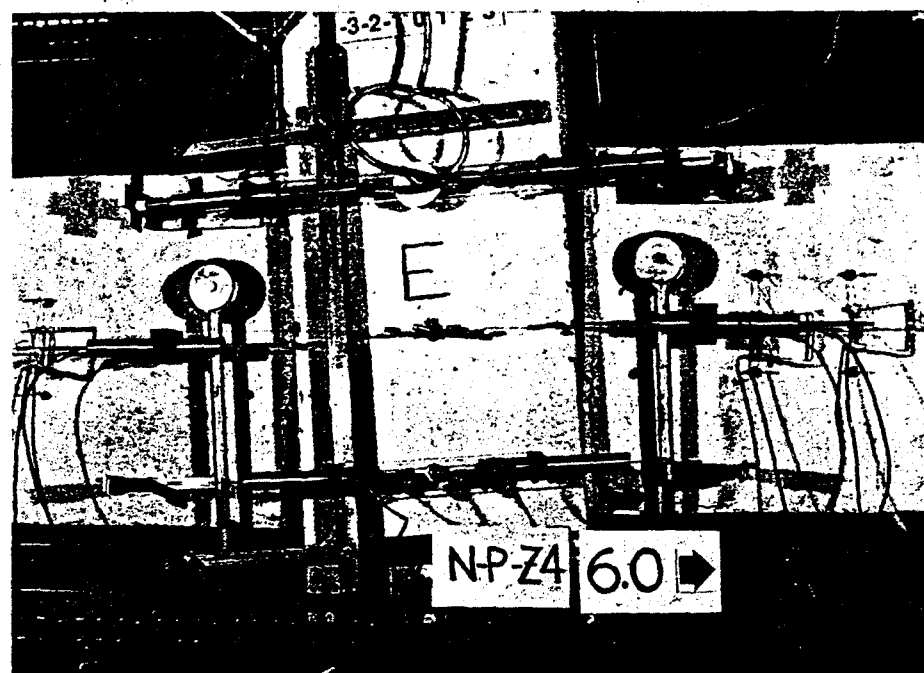Fig. 21—N-P-Z4 at failure (2.9 percent story drift)

Fig. 22—N-P-Z4 at 5.9 percent story drift

PT steel between 105 and 210 MPa (15.2 and 30.5 ksi) based on a modulus of elasticity of 200,000 MPa (29,000 ksi). The difference in the PT steel stress from the start to the end of the test is 130 MPa (18.9 ksi or $0.07 f_{pu}$), which is within the range stated. One possible reason for the existence of the gap was debris falling between the beam and column during the test. Another possible reason is that, upon fracturing, the two pieces of the elongated mild steel bar were misaligned and, as a result, kept the gap between the beam and column from closing totally at zero displacement. This is plausible because the stress increase in the PT steel at zero displacement began after fracture of the mild steel bars occurred.

Story drift—The hysteresis plots for the specimens are given in Fig. 27 through 31. The hysteresis plot for one of the monolithic specimens is given in Fig. 31 for purposes of comparison. The story drifts at failure for all specimens are given in Table 4.

As Table 4 shows, the Phase IV-B specimens failed at slightly lower story drifts than did the two monolithic Zone 4 specimens. The lower value for Specimen N-P-Z4 is a result of the bond failure of the mild steel. It is the opinion of the authors that the story drifts for the Phase IV-B specimens would have been slightly higher than those given in Table 4, had these specimens been subjected to the same loading history as the monolithic specimens. The Phase IV-B specimens were subjected to at least four times as many cycles as
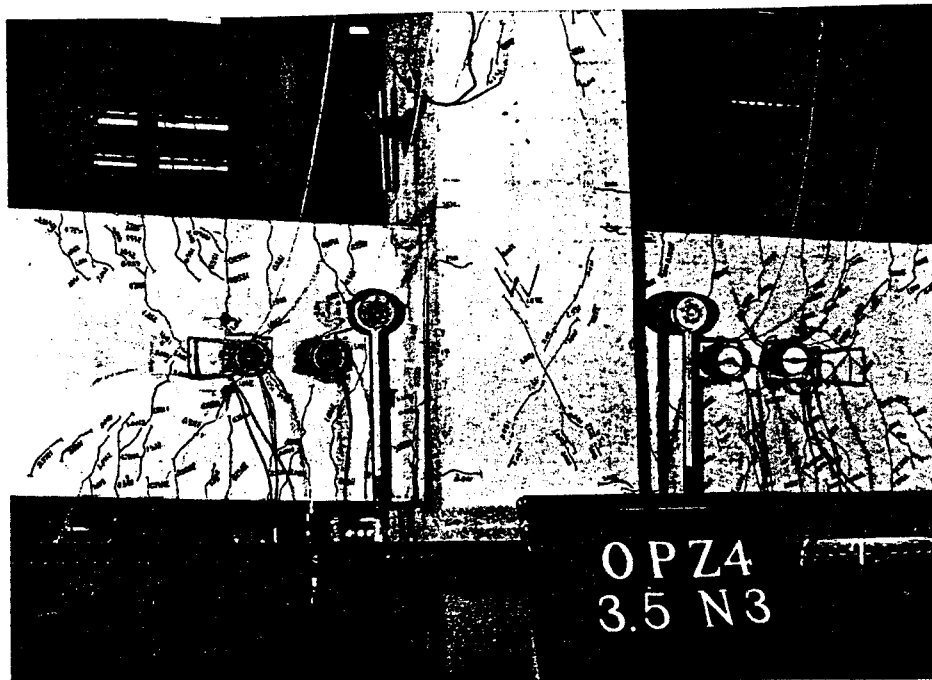
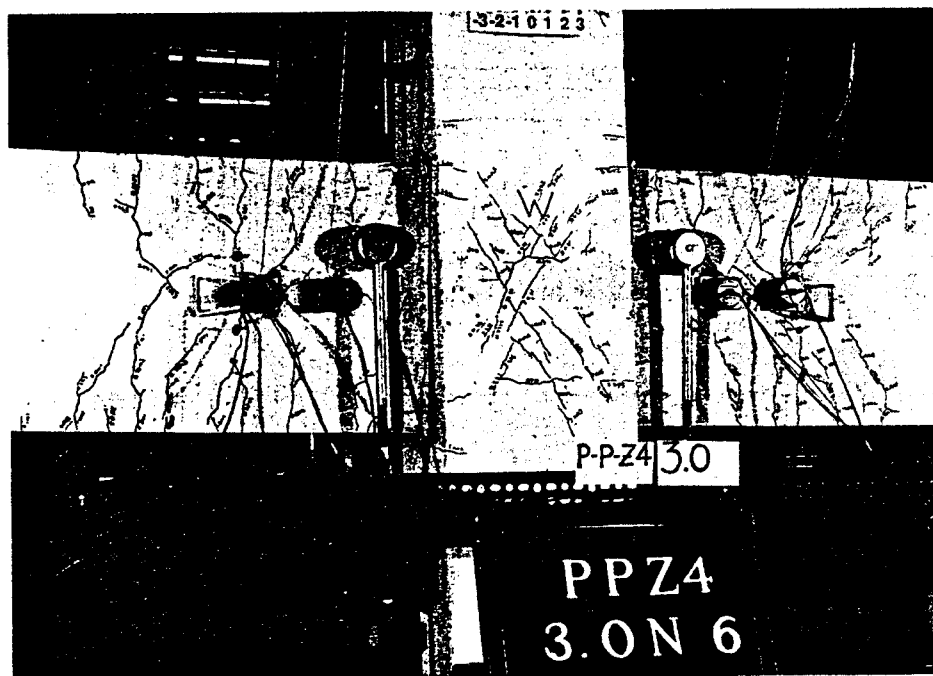*Fig. 23—O-P-Z4 at failure (3.4 percent story drift)*

Fig. 24—P-P-Z4 at failure (2.9 percent story drift in aftershock)

the monolithic Zone 4 specimens.

The definition of failure is subjective. For example, if failure were defined as a drop of 60 percent rather than 80 percent of peak strength, the apparent slight superiority of the monolithic specimens suggested in Table 4 would be eliminated, because all the precast specimens would have reached 6 percent drift without failure. In contrast, the failure for the monolithic specimens would have remained approximately the same. The reason is that the precast specimens suffered almost no concrete damage and could resist the applied shear and undergo large flexural deformations without fracture or loss of anchorage of the PT steel. In contrast, the monolithic specimens were badly damaged and could no longer carry

the shear force. Therefore, the raw values of Table 4 obscure the real major differences in behavior.

Connection strength—The predicted moments given in Table 4 are lower than those for the monolithic Zone 4 specimens because of limitations on the bar and strand sizes available. As Table 4 shows, the average ratio of the experimental moment to the predicted moment was 1.14 and 1.055 for the monolithic and precast specimens, respectively. The smaller value for the precast specimens occurs because a significant amount of their strength is derived from the PT steel, the strength of which is much more closely controlled than that of reinforcing steel.

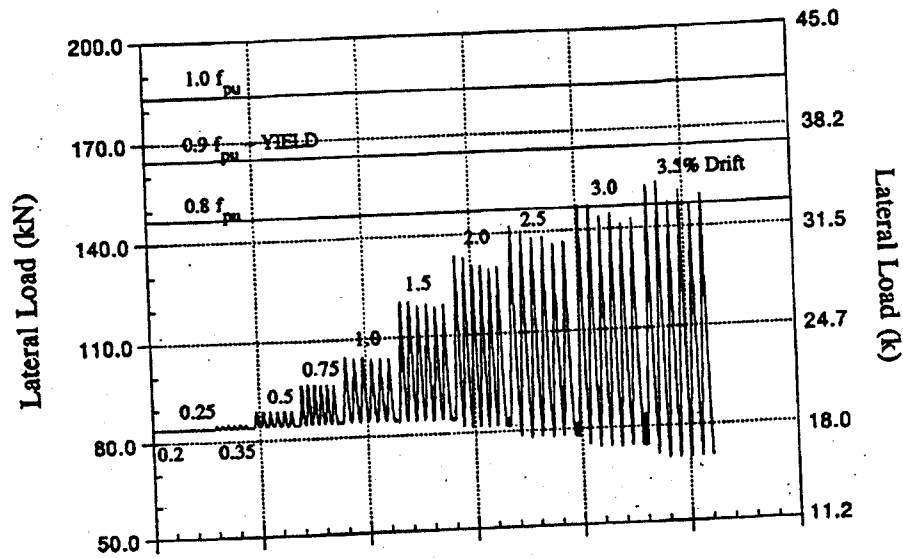*Energy dissipation*—As Fig. 32 shows, the precast speci-

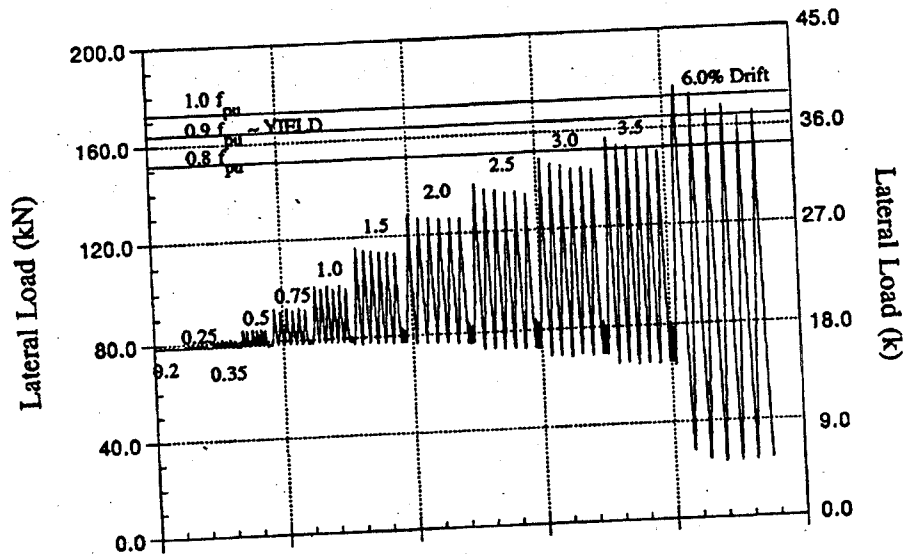Fig. 25—Typical force in prestressing strand, M-P-Z4

Fig. 26—Typical force in prestressing strand, N-P-Z4

mens, except Specimen N-P-Z4, matched the energy dissipation of the monolithic specimen up to approximately 1.5 percent story drift. The code-allowed drift for the prototype structure is approximately 1.1 percent. Fig. 32 shows that the precast specimens dissipated less energy than the monolithic specimen after 1.5 percent story drift. Two points are relevant to the comparison. First, the monolithic specimens were subjected to only one-quarter of the number of cycles that the precast specimens sustained to failure. Under these circumstances, it is unreasonable to expect the same energy dissipation per cycle. Second, recent studies (e.g., Priestley and Tao 1993) have shown that, while some energy dissipation is necessary to control deflections, the benefits at higher drift levels are unclear. This is because the displacements of the structure are more strongly influenced by the individual characteristics of the earthquake and the instantaneous natural period of the structure than by the amount of energy dis-

sipated.

The effects of changing the amount or type of mild steel can be evaluated by comparing suitable specimen pairs. The premature failure by debonding of Specimen N-P-Z4 was unfortunate because it left only one pair of specimens for each comparison.

Specimens M-P-Z4 and O-P-Z4 illustrate the effect of increasing the area of the mild steel by 50 percent. The predicted and experimental flexural strengths increased by almost exactly the same amount, which suggest consistency of behavior. The energy dissipated per cycle changed by an insignificant amount below 1.5 percent drift. However, for drifts greater than 1.5 percent, the energy dissipation increased by approximately 50 percent.

The influence of material type is shown by comparing Specimens O-P-Z4 and P-P-Z4. Because both bar types had approximately the same yield force, they expected to dissi-
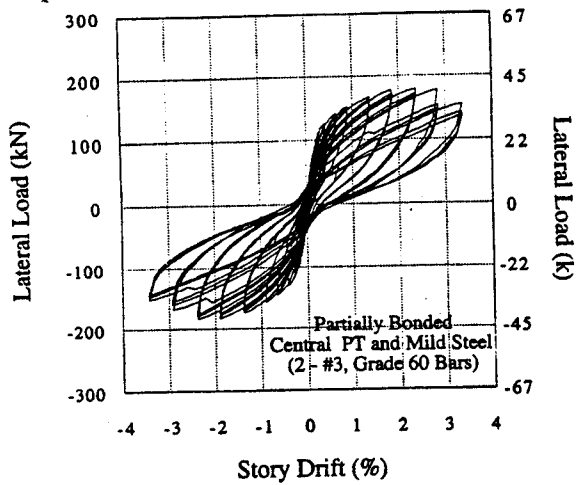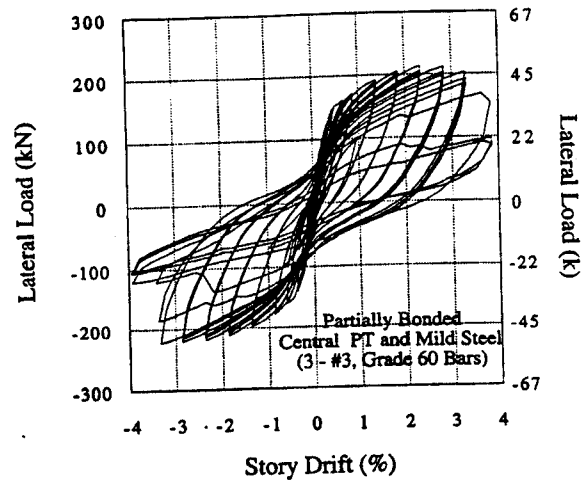
Fig. 27—Hysteresis curves for M-P-Z4
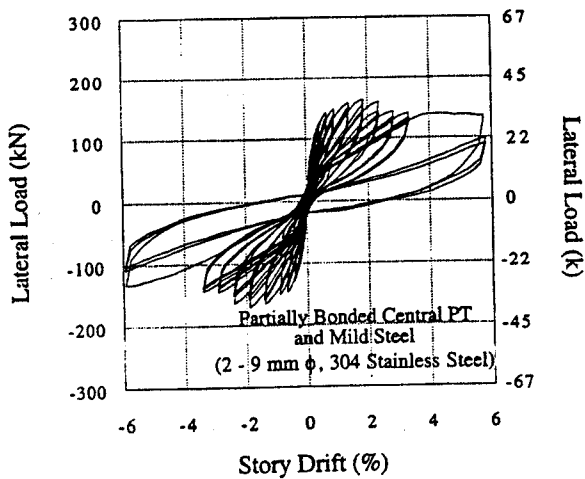

Fig. 28—Hysteresis curves for N-P-Z4

Fig. 29—Hysteresis curves for O-P-Z4

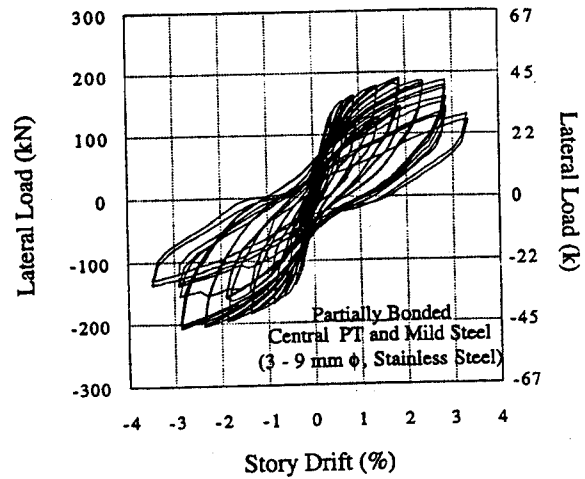
Fig. 30—Hysteresis curves for P-P-Z4

Fig. 31—Hysteresis curves for A-M-Z4

pate the same amount of energy during the same imposed displacement history. Fig. 32 confirms that this was approximately true, although the Grade 60 bars dissipated slightly more energy at drifts greater than 1.5 percent. The stainless steel was expected to sustain larger elongations before failure, but evaluating whether or not it did is made difficult by the fact that the specimens were subjected to different displacement histories.

The shape of the lugs on the stainless steel bars probably influenced their behavior, since the bars fractured at the root of the lug both in the beam-column test and in a separate tension test. In the latter, the elongation was only 30 percent, compared with 55 percent, for an unmachined bar. A 51-mm (2-in.) gage length was used for both. Hot-rolling the lugs on the bar would likely introduce lower stress concentrations and lead to better performance. The authors believe that there is reason to pursue further the design of stainless steel bars for use in precast systems.

CODE IMPLICATIONS

The Uniform Building Code (ICBO 1991) permits only certain building systems to be used in seismic regions. Precast building systems are not included among them. The only
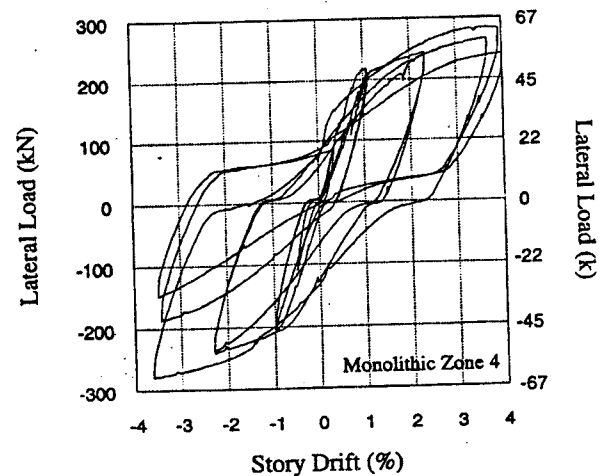
candidate category is reinforced concrete special moment frames, but the proposed hybrid system does not comply with some of the requirements for that category, specifically: 1) the hybrid system uses steel with a yield strength higher than 538 MPa (78 ksi) [UBC 2625 (c) 6]; 2) the beams include bar splices located within $2d$ of the column face; and
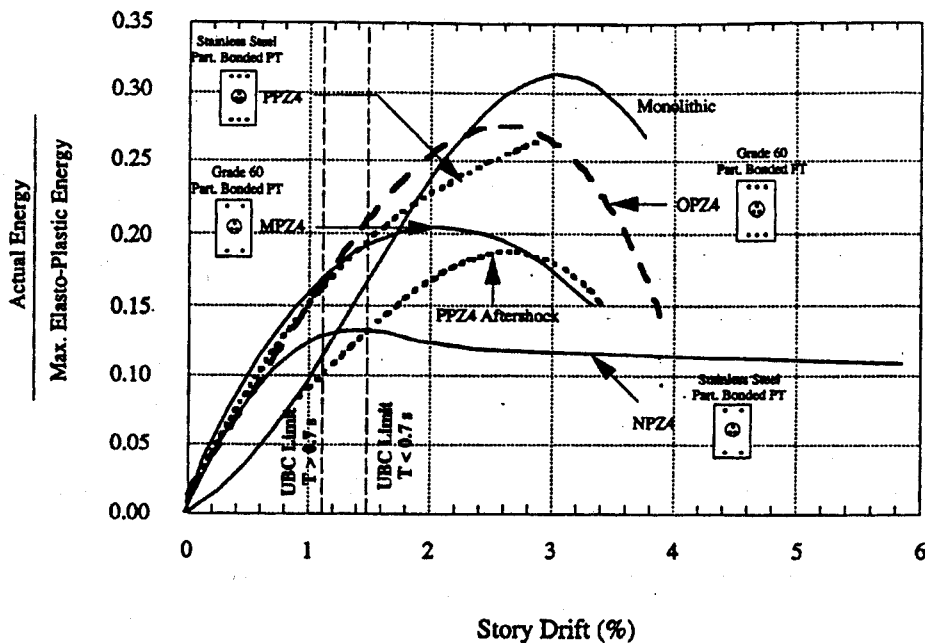
Fig. 32—Comparison of normalized energy dissipated by Phase IV-B specimens

3) the transverse reinforcement needed in the beams and column joint may be less than specified.

The hybrid system may thus be used only under the guise of an "undefined structural system" which must "demonstrate the lateral force resistance and energy absorption capacity to be equivalent to systems" such as a conventionally reinforced concrete system (ICBO 1991). The tests reported here demonstrate the requisite equivalence without question up to a drift of 1.5 percent. At drifts greater than 1.5 percent, the best precast specimen dissipated 75 percent of the energy in the monolithic specimen, but all other characteristics, such as strength retention, stiffness, and structural damage, were superior. The tests, therefore, constitute ample evidence that field performance would be as good as or better than that of a conventional ductile frame.

The exclusion of the use of prestressing steel to resist earthquake-induced forces has now been somewhat relaxed in some codes [e.g., NEHRP 1991, BOCA 1993, and Standard Building Code (SBC) 1994]. Prestressing steel is now allowed to contribute one-quarter of the resistance due to earthquake-induced loads (NEHRP 1991). However, this provision as is and the provision in these codes limiting the amount of prestress to 2.4 MPa (350 psi) would still cause the hybrid system to be noncompliant.

In the long run, provisions of codes such as ACI 318 (1989), UBC (ICBO 1988 and 1991), and NEHRP (1991) that prevent the use of the hybrid system should be modified to permit it. In the short run, a product approval is being sought from ICBO to permit the use of the hybrid system in specific cases. The current acceptance criteria for that approval contains an inconsistency that places a significant burden on new systems: they must sustain cyclic-imposed displacements of ± 4 percent drift without significant degradation of strength and stiffness. This means that to be acceptable to ICBO, a new system must satisfy a standard that a

ductile special moment-resisting frame (SMRF) has been shown to be incapable of attaining, yet the ductile SMRF is the UBC's flagship system to which the new system is meant to be equivalent. A lower drift limit, on the order of 2.5 to 3.0 percent, would be more reasonable.

CONCLUSIONS

The results of 10 tests on precast concrete beam-column connections are reported. The specimens were reinforced with various combinations of bonded and unbonded mild steel and prestressing steel. Two comparable specimens from a previous test series, conventionally reinforced in accordance with UBC requirements for Zone 4, were included for reference. The most highly developed versions of the hybrid system displayed behavior that was in almost every way superior to that of the conventionally reinforced specimens.

1. A hybrid precast system can be designed to have the same flexural strength as a conventionally reinforced system with the same beam size. Prior to fracture of the bars, the hybrid system suffered no strength degradation. The ratio of M_{exp}/M_{pred} was 1.055 and 1.14 for the hybrid and conventional systems, respectively. The former value is smaller because the quality control is tighter on prestressing steel than reinforcing bars.

2. The hybrid system is self-centering and displays essentially no residual drift.

3. The hybrid system has a very large drift capacity. It can undergo load cycles to ±6 percent drift while maintaining 55 percent of its maximum strength.

4. The hybrid system dissipates more energy per cycle than the conventional system up to 1.5 percent drift. Thereafter, the ratio of energy dissipated is approximately 75 percent of the conventional system.

5. The concrete in the hybrid suffered negligible damage, even at drifts up to 6 percent. In the Phase IV-B specimens,

no cracks reached 1-mm (0.04-in.) width; the cracks closed completely when the load was removed. Only minor concrete spalling was found in the cover concrete at the corner angle.

6. The strains in the transverse steel remained below 0.15 f_y, and no sign of shear distress could be detected. This behavior contrasted strongly with that of the conventional specimens which suffered severe shear cracking and were beyond repair at the end of the tests.

7. The use of custom-made WRG (welded reinforcement grids) for transverse reinforcement allowed the cages to be assembled quickly and accurately.

RECOMMENDATIONS FOR FUTURE RESEARCH

Guidelines are currently being prepared for the design of the hybrid precast beam-column connections. These will be based on the experimental test results presented in this paper and the findings from the dynamic analyses, as mentioned in the following. Other areas of necessary research include:

1. Nonlinear dynamic analyses on models that reflect the properties of the physical system are needed to verify the performance under earthquakes rather than pseudo-static loading. Some have been completed (Priestley and Tao 1993, Mole 1994). Others are underway at NIST.

2. Shaking table tests to verify the performance predicted in the preceding.

3. Cyclic load tests on reinforcing bars grouted into ducts to establish their bond properties.

NOTATION

A_g	=	gross area of column
A_s'	=	area of compressive steel
A_{ps}	=	area of PT steel
b	=	width of beam
c	=	neutral axis depth
f_c'	=	concrete compressive stress
f_p	=	stress in PT steel
f_{pe}	=	effective stress in PT steel
f_{pu}	=	nominal stress of PT steel
f_{py}	=	yield stress of PT steel
f_s	=	stress in mild steel
f_y	=	steel yield stress
M_{exp}	=	measured maximum experimental moment
M_{pred}	=	predicted moment
M_n	=	nominal moment
M_u	=	factored moment
V_n	=	nominal shear
V_u	=	factored shear
β_1	=	factor related to concrete strength
ϕ	=	strength reduction factor
λ	=	correction related to unit weight of concrete
μ	=	coefficient of friction
ρ	=	reinforcing ratio

REFERENCES

ACI Committee 318, 1989. "Building Code Requirements for Reinforced Concrete and Commentary (ACI 318-89/ACI 318R-89)," American Concrete Institute, Detroit, 353 pp.

ASTM, 1988. *Annual Book of ASTM Standards*, V. 01.04, American Society of Testing and Materials, Philadelphia.

BOCA, 1993. "National Building Code," Building Officials and Code Administrators International Inc., Country Club Hills.

Cheok, G. S., and Lew, H. S., 1990. "Performance of 1/3-Scale Model Precast Concrete Beam-Column Connections Subjected to Cyclic Inelastic Loads," NISTIR 4433, NIST, Gaithersburg, October.

Cheok, G. S., and Lew, H. S., 1991. "Performance of 1/3-Scale Model Precast Concrete Beam-Column Connections Subjected to Cyclic Inelastic Loads—Report No. 2," NISTIR 4589, NIST, Gaithersburg, June.

Cheok, G.; Stone, W.; and Lew, H. S., 1992. "Partially Prestressed and Debonded Precast Concrete Beam-Column Joints," Proceedings of the 3rd Meeting of the U.S.-Japan Joint Technology Coordinating Committee on Precast Seismic Structures Systems, November.

Cheok, G., and Lew, H. S., 1993. "Model Precast Concrete Beam-to-Column Connections Subject to Cyclic Loading," *PCI Journal*, Precast/Prestressed Concrete Institute, Chicago, July/Aug., pp. 80-92.

Cheok, G. S., and Stone, W. C., 1993. "Performance of 1/3-Scale Model Precast Concrete Beam-Column Connections Subjected to Cyclic Inelastic Loads—Report No. 3," NISTIR 5246, NIST, Gaithersburg, August.

Cheok, G. S., and Stone, W. C., 1994. "Performance of 1/3-Scale Model Precast Concrete Beam-Column Connections Subjected to Cyclic Inelastic Loads—Report No. 4," NISTIR 5436, NIST, Gaithersburg, June.

Darwin, D., and Graham, E. K., 1993. "Effect of Deformation Height and Spacing on Bond Strength of Reinforcing Bars," *ACI Structural Journal*, V. 90, No. 6, Nov.-Dec., pp. 646-657.

International Conference of Building Officials (ICBO), 1988, 1991. Uniform Building Code, Whittier, CA.

Mole, A., 1994. "Seismic Response of Hybrid Connections in Precast Concrete Frames," master's thesis, University of Washington, December.

NEHRP, 1991. "Recommended Provisions for the Development of Seismic Regulations for New Buildings," Part 1, Federal Emergency Management Agency, Washington, D. C.

Priestley, M. J. N., and Tao, J. R., 1993. "Seismic Response of Precast Prestressed Concrete Frames with Partially Debonded Tendons," *PCI Journal*, V. 38, No. 1, Jan.-Feb., pp. 58-69.

Priestley, M. J. N., ed., 1992. "Report on the Third U.S. PRESSS Coordinating Meeting," *Report* No. PRESSS-92/02, Department of Applied Mechanics and Engineering Sciences, UCSD, La Jolla, Aug., pp. 12-26.

SBC, 1994. "Standard Building Code," Southern Building Code Congress International Inc., Birmingham.